Precise measurement of a weak radio frequency electric field using a resonant atomic probe*

Liping Hao(郝丽萍)¹, Yongmei Xue(薛咏梅)¹, Jiabei Fan(樊佳蓓)¹, Jingxu Bai(白景旭)¹, Yuechun Jiao(焦月春)^{1,2}, and Jianming Zhao(赵建明)^{1,2,†}

¹ State Key Laboratory of Quantum Optics and Quantum Optics Devices, Institute of Laser Spectroscopy, Shanxi University, Taiyuan 030006, China

² Collaborative Innovation Center of Extreme Optics, Shanxi University, Taiyuan 030006, China

(Received 26 November 2019; revised manuscript received 9 January 2020; accepted manuscript online 16 January 2020)

We present a precise measurement of a weak radio frequency electric field with a frequency of \lesssim 3 GHz employing a resonant atomic probe that is constituted with a Rydberg cascade three-level atom, including a cesium ground state $|6S_{1/2}\rangle$, an excited state $|6P_{3/2}\rangle$, and Rydberg state $|nD_{5/2}\rangle$. Two radio frequency (RF) electric fields, noted as local and signal fields, couple the nearby Rydberg transition. The two-photon resonant Rydberg electromagnetically induced transparency (Rydberg-EIT) is employed to directly read out the weak signal field having hundreds of kHz difference between the local and signal fields that is encoded in the resonant microwave-dressed Rydberg atoms. The minimum detectable signal fields of $E_{S_{min}} = 1.36 \pm 0.04$ mV/m for 2.18 GHz coupling $|68D_{5/2}\rangle \rightarrow |69P_{3/2}\rangle$ transition and 1.33 ± 0.02 mV/m for 1.32 GHz coupling $|80D_{5/2}\rangle \rightarrow |81P_{3/2}\rangle$ transition are obtained, respectively. The bandwidth dependence is also investigated by varying the signal field frequency and corresponding -3 dB bandwidth of 3 MHz is attained. This method can be employed to perform a rapid and precise measurement of the weak electric field, which is important for the atom-based microwave metrology.

Keywords: Rydberg electromagnetically induced transparency (Rydberg-EIT), atomic probe, weak field mea-

surement

PACS: 32.80.Ee, 42.50.Gy, 84.40.–x

1. Introduction

Precise measurements of a weak radio frequency field with frequency less than 3 GHz play an important role in science, communication, and everyday life. Rydberg atombased electric field sensor has achieved great progress in recent years due to its large electric polarizability ($\propto n^7$) and big microwave-transition dipole moments ($\propto n^2$).^[1] It covers the frequency range over from megahertz to terahertz, and has a potential to outperform the traditional electrometry due to the self-calibration characteristics. An all-optical sensing method based-on Rydberg electromagnetically induced transparency (Rydberg-EIT)^[2] and Autler–Townes (AT) splitting^[3] has been employed to character the properties of electric fields, including the measurements of microwave fields magnitude, [4-6] polarization, [7,8] phase, [9] as well as millimeter waves, [10] static electric fields, [11,12] subwavelength imaging of microwave electric-field distributions, [13,14] field inhomogeneities, [15,16] and nonlinearity. [17] Rydberg atoms have been also used as a radio frequency receiver for retrieving amplitude modulated (AM) base band signals that result in the "Rydberg atom radio" [18-20] and can also be used to realize the extension of the feasibility of digital communication via a continuously tunable radio-frequency carrier.

A few techniques have been proposed for improving the

sensitivity of weak field measurements, for example, (i) using high fineness optical cavities to narrow the EIT linewidth for improving the AT splitting resolution; (ii) using Mach-Zehnder interferometer detection^[21] and a frequency modulation technique^[22] to increase the signal-to-noise ratio; (iii) a Rydberg atom-based mixer has been used to realize the weak electric-field detection with sub-Hz resolution for the microwave field. [23,24] In this work, we present a precise measurement of weak electric field in a room-temperature cesium vapor cell, where an atomic probe is employed to directly readout the weak radio frequency field that is encoded in the local microwave field. The RF field frequency of $\sim 2.18~\text{GHz}$ $(\sim 1.32\,\text{GHz})$ couples a nearby Rydberg transition $|68D_{5/2}\rangle$ \rightarrow $|69P_{3/2}\rangle$ ($|80D_{5/2}\rangle \rightarrow |81P_{3/2}\rangle$). The frequency of the weak signal electric field is hundreds of kHz different from the local field. The Rydberg-EIT is employed to directly detect the weak signal field, the corresponding minimum detectable field is $\sim 1.36 \pm 0.04$ mV/m $(1.33 \pm 0.02$ mV/m) with a -3 dB measurement bandwidth of 3 MHz.

2. Experimental setup

DOI: 10.1088/1674-1056/ab6c49

Experiments are implemented in a room-temperature cesium cell of length 50 mm and diameter 20 mm, as shown in Fig. 1(a), and the relevant Rydberg EIT-AT four-level di-

^{*}Project supported by the National Key R&D Program of China (Grant No. 2017YFA0304203), the National Natural Science Foundation of China (Grant Nos. 61475090, 61675123, 61775124, and 11804202), the State Key Program of National Natural Science of China (Grant Nos. 11434007 and 61835007), and Changjiang Scholars and Innovative Research Team in University of Ministry of Education of China (Grant No. IRT_17R70).

[†]Corresponding author. E-mail: zhaojm@sxu.edu.cn

agram is given in Fig. 1(b). A probe and a coupling lasers overlap and counter-propagate through the cell. The weak probe beam, $\lambda_p=852$ nm, is produced by an external cavity diode laser (Toptica DLpro) with a $1/e^2$ waist of 100 μ m at the cell center. The probe frequency is locked to the transition $|6S_{1/2}F=4\rangle \rightarrow |6P_{3/2}F'=5\rangle$ using a super stable optical cavity (1.5 GHz FSR and 15000 fineness). The strong coupling laser, $\lambda_c=510$ nm, is originated from a commercial laser (Toptica SHG110) with a $1/e^2$ waist of 172 μ m at the cell center, related frequency locked to the $|6P_{3/2}F'=5\rangle \rightarrow |68D_{5/2}\rangle$ Rydberg transition. Two radio frequency fields, denoted as

local $(E_{\rm L})$ and weak signal $(E_{\rm S})$ fields with hundreds of kHz frequency difference, interact with the atoms simultaneously. Due to the small frequency difference between the two radio frequency fields and the small amplitude of the signal field, the electric field that atoms experienced is considered as the modulation of the local field, [19] see details below. The power of the probe beam passing through the cell is detected with a photodiode (PD) and recorded with an oscilloscope. Both radio frequency electric fields have the polarization along z axis and parallel to the polarization of the probe and coupling beams.

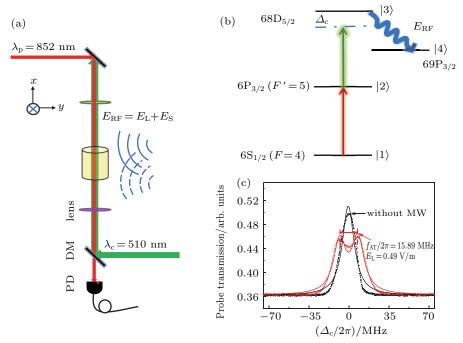


Fig. 1. (a) Schematic diagram of experiments. The coupling and probe beams, forming a Rydberg three-level system, counter-propagate through a cesium vapor cell along the x axis. Two radio frequency fields with hundreds of kHz difference, denoted with solid and dashed arcs, interact with the three-level system. The one radio frequency field is denoted as a local field (E_L) and the other one as a weak signal field (E_S) . The transmission of the probe is used to directly read out the signal field by a photodiode (PD) after a dichroic mirror (DM). (b) Energy level diagram. The probe (coupling) laser is resonant with the lower $|6S_{1/2}F = 4\rangle \rightarrow |6P_{3/2}F' = 5\rangle$ (up $|6P_{3/2}F' = 5\rangle \rightarrow |68D_{5/2}\rangle$) transition. The local (signal) field with the frequency ~ 2.18 GHz couples Rydberg transition $|68D_{5/2}\rangle \rightarrow |69P_{3/2}\rangle$. Small frequency difference between the two radio frequency fields results in the modulation to the local field, see text. (c) Measurements of Rydberg EIT-AT spectra as a function of the coupling laser detuning Δ_c with a local field $E_L = 0.49$ V/m. The solid lines correspond to Lorentz fittings to the EIT-AT spectra. The extracted EIT linewidth is $T_{\rm EIT} = 2\pi \times (12.54 \pm 0.13)$ MHz. The coupling frequency is continuously scanned by the SC110 module of a commercial laser Toptica SHG110 and the probe transmission spectrum is detected by a PD and recorded with an oscilloscope.

A local radio frequency field, generated with a function generator (SRS SG384) and emitted from a horn antenna, is applied transversely to the laser beams propagating through the vapor cell, where it interacts with cesium Rydberg atoms. The local field has a frequency ~ 2.18 GHz (1.32 GHz), resonantly driving the $|68D_{5/2}\rangle \rightarrow |69P_{3/2}\rangle$ ($|80D_{5/2}\rangle \rightarrow |81P_{3/2}\rangle$) Rydberg transition with Rabi frequency Ω_{RF} . A signal field with hundreds of kHz difference in frequency from the local field, is originated from another function generator (Keysight N5183B) and emitted by another antenna. The local field causes an AT splitting of the Rydberg-EIT illustrated in Fig. 1(c) as a function of the coupling laser detuning. The Lorentz fitting to the field-free EIT spectrum yields linewidth

 $\Gamma_{\rm EIT}=2\pi imes (12.54\pm0.13)$ MHz. An observed EIT transmission splits into two peaks, EIT-AT splitting $f_{\rm AT}$, in the presence of local field $E_{\rm L}$. Analysis of the Rydberg-EIT-AT spectra reveals the $\Omega_{\rm RF}$ value, which is proportional to the radio frequency electric field. Hence, this spectroscopic method affords an all-optical readout of the time-dependent field strength. The extracted $f_{\rm AT}$ is $2\pi imes 15.89$ MHz by using multi-peak Lorentz fittings to the data (red solid line), corresponding local electric field $E_{\rm L}=0.49$ V/m. In following experiments of weak signal field measurements, the local field is set to this value. The coupling laser frequency is locked to the up transition $|6P_{3/2}F'=5\rangle \rightarrow |68D_{5/2}\rangle$ ($|80D_{5/2}\rangle$) and the Rabi frequencies of the probe and coupling beams are

 $\Omega_{\rm p} = 2\pi \times 13.35$ MHz and $\Omega_{\rm c} = 2\pi \times 2.94$ MHz, respectively.

3. Results and discussion

Microwave field measurement based on Rydberg EIT-AT splitting is no longer applicable for the weak electric field when the field induced AT splitting is less than the EIT linewidth, $f_{\rm AT} \lesssim \Gamma_{\rm EIT}$. To detect the weak field, we encode this weak field, considered as a signal field $E_{\rm S} = E_{\rm S}' \cos(\omega_{\rm S} t + \phi_{\rm S})$, to a strong local field $(E_{\rm L} = E_{\rm L}' \cos(\omega_{\rm L} t + \phi_{\rm L}))$. Both the weak signal and strong local fields incident on to the vapor cell simultaneously. Such that the radio frequency field the atoms experienced in the path of the probe and coupling beams is written as

$$E_{\rm RF} = E_{\rm L} + E_{\rm S}.\tag{1}$$

For the signal field with its polarization being parallel to the local field and the frequency difference satisfying the condition of $\Delta\omega=\omega_L-\omega_S\ll\bar{\omega},\;\bar{\omega}=\frac{\omega_L+\omega_S}{2},$ the scalar total microwave electric field that the atoms feel can be expressed as

$$|E_{\rm RF}| = \sqrt{E_{\rm L}'^2 + E_{\rm S}'^2 + 2E_{\rm L}'E_{\rm S}'\cos(\Delta\omega t + \Delta\phi)},$$
 (2)

with $\omega_L = 2\pi f_L$, and $\omega_S = 2\pi f_S$, $\Delta \phi = \phi_L - \phi_S$. For the weak signal field, $E_S' \ll E_I'$, equation (2) is further simplified as

$$|E_{\rm RF}| \approx E_{\rm L}' + E_{\rm S}' \cos(\Delta \omega t + \Delta \phi).$$
 (3)

Equation (3) demonstrates that the radio frequency field the atoms experienced is regarded as the local field that is encoded or modulated by a baseband signal of the modulation frequency $\Delta \omega$ and amplitude $E_{\rm S}'$, which results in a modulation of the EIT spectrum. The amplitude of the weak signal field $E_{\rm S}'$ can be directly optically read out. [19]

The probe-power transmission is $P=P_0\exp(-\alpha L)$, with the probe-laser absorption coefficient $\alpha=2\pi {\rm Im}(\chi)/\lambda_{\rm p}$ and L the vapor cell length. The χ is the susceptibility of the medium seen by the probe laser. The χ is written as

$$\chi = \frac{2N\mu_{12}}{E_{\rm p}\varepsilon_0}\rho_{12},\tag{4}$$

with N the average atomic density, μ_{12} (ρ_{12}) the dipole moment (the density matrix element) of transition $|1\rangle \rightarrow |2\rangle$, E_p the amplitude of the probe, and ε_0 the vacuum permittivity. For the four-level atoms denoted in Fig. 1(b), $\chi(\rho_{12})$ displays the EIT-AT spectrum when we scan the probe or coupling laser frequency, as shown in Fig. 1(c). However for the case of the two-photon resonant Rydberg-EIT, the probe transmission strongly depends on the radio frequency field. The χ is a function of the radio frequency electric field $|E_{RF}|$, where the corresponding probe transmission is proportional to the magnitude of the radio frequency electric field. The probe transmission detected by the photodiode detector is taken as

$$P \propto |E_{RF}| \approx E'_{L} + E'_{S} \cos(\Delta \omega t + \Delta \phi).$$
 (5)

It is found from Eq. (5) that the detected probe transmission at EIT resonance is varied with frequency $\Delta \omega = \omega_L - \omega_S$ (difference between signal and local field frequencies), related amplitude proportional to the signal field E_S' .

In a preliminary experimental test, we set local field frequency $\omega_L = 2\pi \times 2.185740$ GHz that couples the nearby Rydberg transition $|68D_{5/2}\rangle \rightarrow |69P_{3/2}\rangle$. The local field results in the AT splitting, $f_{\rm AT} = 2\pi \times 15.89$ MHz, that is close to the EIT linewidth, see Fig. 1(c). The weak signal field frequency $\omega_{\rm S} = 2\pi \times 2.185780$ GHz with frequency difference $\Delta \omega = 2\pi \times 40$ kHz relative to the local field. Figure 2 presents the measured probe laser transmission for three indicated radio frequency $E_{\rm S}$ fields under two photon resonant Rydberg-EIT. The probe laser transmission shows a nice sinusoidal profile with a frequency 40 kHz. We fit the spectra of Fig. 2 with sine function to extract the amplitude E'_{S} . It is clearly shown that the probe transmission amplitude decreases when the signal intensity E_S decreases, the corresponding signal fields are 0.08 V/m, 0.13 V/m, and 0.18 V/m, respectively. The values of electric field can be acquired by calibrating the probe transmission amplitude with an EIT-AT spectrum discussed below.

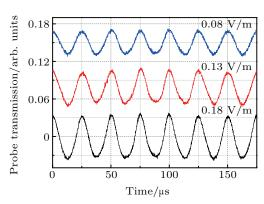


Fig. 2. Measurements of the probe laser transmission with an indicated weak signal field $E_{\rm S} = 0.18$ V/m (bottom), 0.13 V/m (middle), 0.08 V/m (top) in the presence of the local field $E_{\rm L} = 0.49$ V/m at two photon resonant Rydberg-EIT. The transmission shows a nice sinusoidal profile, the related amplitude increases with the signal field $E_{\rm S}$.

When the signal field decreases further, the detected probe transmission displays a deformed sine profile that can not be well fitted with a sine function. To read out the amplitude of weak field $E_{\rm S}$, we employ a lock-in amplifier triggered by the beat signal $E_{\rm S}'\cos(\Delta\omega t + \Delta\phi)$ that is obtained with a radio frequency mixer. The output of the lock-in amplifier is proportional to the amplitude of signal field $E_{\rm S}$. To do the test, we decrease the signal electric field and do a series of measurements, corresponding electric fields displayed with red squares in Fig. 3(a) for $\omega_{\rm L} \sim 2\pi \times 2.18$ GHz. The inset of Fig. 3(a) displays the output of the lock-in amplifier. To calibrate the electric field value, we use the Rydberg EIT-AT spectra at strong field range with the formula $f_{\rm AT} = \Omega_{\rm RF} = \mu E_{\rm RF}/\hbar$, in which $\Omega_{\rm RF}$ (μ) denotes the Rabi frequency (dipole matrix element) the radio frequency field coupled and \hbar is the reduced Planck

constant. The measured strong electric field is shown with blue circles in Fig. 3(a). The radio frequency field is proportional to the square root of the output power of the function generator^[25]

$$E_{\rm RF} = \sqrt{30 P_{\rm RF} g} / d, \tag{6}$$

with g the gain of the antenna and d the distance from the antenna to the vapor cell. Equation (6) is plotted with a black solid line in Fig. 3(a). The EIT-AT splittings at strong field together with Eq. (6) are used to calibrate the measurements of Figs. 2 and 3. The measurements of Fig. 3(a) demonstrates the strong field together with Eq. (6) are used to calibrate the measurements of Figs. 3 (a) demonstrates the strong field together with Eq. (6) are used to calibrate the measurements of Figs. 3 (a) demonstrates the strong field together with Eq. (6) are used to calibrate the measurements of Figs. 3 (a) demonstrates the strong field together with Eq. (6) are used to calibrate the measurements of Figs. 3 (a) demonstrates the strong field together with Eq. (6) are used to calibrate the measurements of Figs. 3 (a) demonstrates the strong field together with Eq. (6) are used to calibrate the measurements of Figs. 3 (a) demonstrates the strong field together with Eq. (6) are used to calibrate the measurements of Figs. 3 (a) demonstrates the strong field together with Eq. (6) are used to call the strong field together with Eq. (7) and (8) are used to call the strong field together with Eq. (8) are used to call the strong field together with Eq. (9) are used to call the strong field together with Eq. (9) are used to call the strong field together with Eq. (9) are used to call the strong field together with Eq. (9) are used to call the strong field together with Eq. (9) are used to call the strong field together with Eq. (9) are used to call the strong field together with Eq. (9) are used to call the strong field together with Eq. (9) are used to call the strong field together with Eq. (9) are used to call the strong field together with Eq. (9) are used to call the strong field together with Eq. (9) are used to call the strong field together with Eq. (9) are used to call the strong field together with Eq. (9) are used to call the strong field together with Eq. (9) are used to call the strong field together with

strate a linear dependence on $\sqrt{P_{RF}}$, corresponding slope parallel to the calculation, from which the radio frequency field is extracted. The last point in the linear line yields the detectable minimum value $E_{S_{min}}=1.36\pm0.04$ mV/m for 2.18-GHz singal field (Fig. 3(a)), the related error bars display the standard error of two independent measurements. To verify this method, we change the local field frequency to 1.32-GHz that couples the $|80D_{5/2}\rangle \rightarrow |81P_{3/2}\rangle$ Rydberg transition and do similar measurements, the corresponding results are shown in Fig. 3(b). The achieved minimum detectable field of $E_{S_{min}}=1.33\pm0.02$ mV/m.

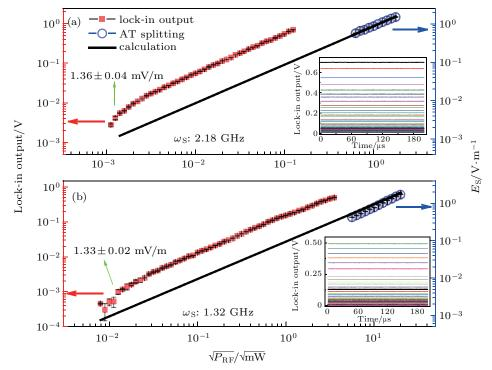


Fig. 3. Measurements of the lock-in output of the probe transmission (red squares) and signal fields $E_{\rm S}$ (blue circles) by EIT-AT spectra versus the square root of the output power, $\sqrt{P_{\rm RF}}$, of the function generator for (a) signal field frequency $\omega_{\rm S}\sim 2\pi\times 2.18$ GHz and (b) $\omega_{\rm S}\sim 2\pi\times 1.32$ GHz. The black line is the calculation of equation $E_{\rm RF}=\sqrt{30P_{\rm RF}g}/d$. The detectable minimum of signal field $E_{\rm S_{min}}=1.36\pm0.04$ mV/m in (a) and 1.33 ± 0.02 mV/m in (b). The error bars display the standard error of two independent measurements. The inset demonstrates the lock-in output of the probe transmission.

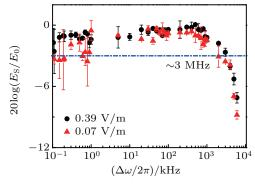


Fig. 4. Measurements of signal electric field, $20\log(E_{\rm S}/E_0)$, as a function of $\Delta\omega$ by changing the signal field frequency for two indicated signal field values $E_{\rm S}=0.39$ V/m (black circles) and 0.07 V/m (red triangles), respectively. Horizontal dot-dashed line displays the idea -3 dB line, related -3 dB bandwidth of 3 MHz, depending on the photodiode used.

Finally, we measure the bandwidth of the signal field. We change the frequency of the signal field while keep the local

field fixed and do the similar measurements of Fig. 3. Figure 4 presents the measurements of electric field, $20\log(E_{\rm S}/E_0)$, as a function of the signal field frequency for two different field values, $E_{\rm S}=0.39$ V/m (black circles) and 0.07 V/m (red triangles), respectively. The -3 dB bandwidth is about 3 MHz, which depends on the photodiode detector used.

4. Conclusion

In summary, we have presented a weak electric field measurement for a frequency $\omega_{\rm S} \lesssim 2\pi \times 3$ GHz employing a resonant atomic probe. When the signal field is much weaker than the local field, $E_{\rm S} \ll E_{\rm L}$, the two-photon resonant Rydberg EIT displays a sine profile with frequency difference of the local and signal fields, $\Delta \omega$, and sine amplitude of $E_{\rm S}'$. This sine profile of the probe transmission yields a fast and direct readout

of the signal radio frequency electric field. The measured minimum fields of 1.36 ± 0.04 mV/m and 1.33 ± 0.02 mV/m are attained for two selected test RF frequencies of 2.18 GHz and 1.32 GHz, respectively. The resonant atomic probe provides a method of fast and direct readout the field value without further processing and the related radio frequency easily extends to tens of GHz. Furthermore, this method can be used to measure the radio frequency electric field with signal frequency being continuously varied, arriving at -3 dB bandwidth of 3 MHz in this work. The bandwidth can be a few MHz depending on the optical detector used. The measured accuracy could be improved by one order of magnitude by compressing the laser frequency and intensity noise. Compared to the previous field measurements, [21,22] the method of this work is simple and provides a rapid and precise way to measure the weak radio frequency electric field.

References

- Gallagher T F 1994 Rydberg atom (Cambridge: Cambridge University Press)
- [2] Mohapatra A K, Jackson T R and Adams C S 2007 Phys. Rev. Lett. 98 113003
- [3] Autler S H and Townes C H 1955 Phys. Rev. 100 703
- [4] Holloway C L, Gordon J A, Jefferts S, Schwarzkopf A, Anderson D A, Miller S A, Thaicharoen N and Raithel G 2014 IEEE Trans. Antennas Propag. 62 6169
- [5] Sedlacek J A, Schwettmann A, Kübler H, Löw R, Pfau T and Shaffer J P 2012 Nat. Phys. 8 819
- [6] Holloway C L, Simons M T, Gordon J A, Dienstfrey A, Anderson D A and Raithel G 2017 J. Appl. phys. 121 233106

- [7] Sedlacek J A, Schwettmann A, Kübler H and Shaffer J P 2013 Phys. Rev. Lett. 111 063001
- [8] Koepsell J, Thiele T, Deiglmayr J, Wallraff A and Merkt F 2017 Phys. Rev. A 95 053860
- [9] Simons M T, Haddab A H, Gordon J A and Holloway C L 2019 Appl. Phys. Lett. 114 114101
- [10] Gordon J A, Holloway C L, Schwarzkopf A, Anderson D A, Miller S, Thaicharoen N and Raithel G 2014 Appl. Phys. Lett. 105 024104
- [11] Jiao Y C, Han X X, Yang Z W, Li J K, Raithel G, Zhao J M and Jia S T 2016 Phys. Rev. A 94 023832
- [12] Jiao Y C, Hao L P, Han X X, Bai S Y, Raithel G, Zhao J M and Jia S T 2017 Phys. Rev. Appl. 8 014028
- [13] Fan H Q, Kumar S, Daschner R, Kübler H and Shaffer J P 2014 Opt. Lett. 39 3030
- [14] Holloway C L, Gordon J A, Schwarzkopf A, Anderson D A, Miller S A, Thaicharoen N and Raithel G 2014 Appl. Phys. Lett. 104 244102
- [15] Fan H Q, Kumar S, Sheng J T, Shaffer J P, Holloway C L and Gordon J A 2015 Phys. Rev. Appl. 4 044015
- [16] Zhang L J, Liu J S, Jia Y, Zhang H, Song Z F and Jia S T 2018 Chin. Phys. B 27 033201
- [17] Hao L P, Xue Y M, Fan J B, Jiao Y C, Zhao J M and Jia S T 2019 Appl. Sci. 9 1720
- [18] Cox K C, Meyer D H, Fatemi F K and Kunz P D 2018 Phys. Rev. Lett. 121 110502
- [19] Jiao Y C, Han X X, Fan J B, Raithel G, Zhao J M and Jia S T 2019 Appl. Phys. Exp. 12 126002
- [20] Song Z F, Liu H P, Liu X C, Zhang W F, Zou H Y, Zhang J and Qu J F 2019 Opt. Exp. 27 8848
- [21] Kumar S, Fan H Q, Kübler H, Sheng J T and Shaffer J P 2017 Sci. Rep. 7 42981
- [22] Kumar S, Fan H Q, Kübler H, Jahangiri A J and Shaffer J P 2017 Opt. Exp. 25 8625
- [23] Gordon J A, Simons M T, Haddab A H and Holloway C L 2019 AIP Advances 9 045030
- [24] Holloway C L, Simons M T, Gordon J A and Novotny D 2019 IEEE Antennas and Wireless Propagation Letters 18 1853
- [25] Fan J B, Jiao Y C, Hao L P, Xue Y M, Zhao J M and Jia S T 2018 Acta Phys. Sin. 67 093201 (in Chinese)